Effects of Nickel on the Sintering Behavior of Fe-Ni Compacts Made from Composite and Elemental Powders

K.S. HWANG and M.Y. SHIAU

Injection-molded Fe-Ni parts made from composite and elemental powders were prepared, and the effect of nickel on the sintering of iron compacts was investigated. Dilatometry analyses showed that the alpha-gamma phase transformation temperature of the Fe-Ni compact changed from a fixed 912 °C for pure iron to a temperature range between 700 °C and 912 °C where two phases coexisted. The microstructure indicated that nickel impeded surface diffusion and slowed down the neck growth rate of iron powder in the early sintering stage. The dual phase and the small neck size at low temperatures suppressed the exaggerated grain growth, which usually occurs on carbonyl iron powders at 912 °C. It was also observed that nickel impeded the grain growth of iron at high temperatures. Thus, by reducing the exaggerated grain growth during phase transformation, impeding the grain growth at high temperatures, and with high diffusion rates of iron in Ni-rich areas, enhanced densification was obtained for Fe-Ni systems, particularly for those systems made from composite powders. However, when coarse nickel powder was added, expansion was observed due to the presence of large pores around nickel powders. These pores were formed because of the particle rearrangement which was caused by the Kirkendall effect.

I. INTRODUCTION

NICKEL has been shown to enhance the sintering of iron compacts,[1,2,3] and the degree of enhancement depends on the quantity and the method of its introduction. Since nickel has been known to be a beneficial sintering aid for conventional powder metal iron compacts, it has also been employed since the early development stage of powder injection molding (PIM). Several studies[4,5,6] examined the Fe-Ni system using elemental powder mixtures with the nickel content varied from 0 to 8 wt pct. These studies indicated that nickel could enhance sintering but that its distribution in the microstructure was not uniform. It would be intuitive to think that to improve the homogeneity in microstructure and mechanical properties, fine powders or, even better yet, composite powders would be ideal starting materials. Several studies using the conventional press-and-sinter process have indeed shown that composite Fe-Cu, Fe-Ni, and Fe-Ni-Mo powders give higher sintered densities and better mechanical properties than do mixed powders.[7–10] With this idea in mind, nickel-coated iron powder was also evaluated for PIM by this group, and the results with regard to mechanical properties showed that composite powders produced higher strength and ductility.[11]

One of the explanations for the role of nickel in enhanced sintering of iron compacts is that nickel is present in the grain boundaries of the iron matrix during sintering, which impedes grain growth.[1,10] Another hypothesis is that with nickel present in the grain boundaries, the grain boundary diffusion rate of iron is increased.[9,10] Countering to these benefits of nickel additions, it was also found that Kirkendall porosities formed in the iron side of the Fe-Ni diffusion couple,[12,13] which led to dimensional expansion and poor sintered density for Fe-Ni compacts.

Mitani *et al.*[12] showed that the maximum sintered density was obtained at 2 wt pct Ni for mixed coarse electrolytic iron and electrolytic nickel powders. When more nickel was added, expansion occurred and reached a maximum at 50 wt pct Ni. If fine carbonyl iron powder was used, only densification was noted, and it increased with an increasing amount of nickel. Zhang and German[4] also reported a maximum density at 2 wt pct Ni using the PIM process with 4-μm carbonyl iron powder and 9-μm nickel powder. Kohara and Tatsuzawa[9] used $-100 + 325$ mesh composite powder and the press-and-sinter technique and found that densification increased as nickel content increased. Hanatate[10] used $-150 + 200$ mesh composite powder and noted that the density reached a plateau at 0.08 wt pct. Further addition of nickel did not improve densification. These experiments showed that the method of nickel introduction, the size of the iron and nickel powders, and the processing method used in making the compacts are all critical factors in determining the optimum nickel addition to obtain the maximum sintered density of Fe-Ni compacts.

The effect of nickel coating on sintered densities and the mechanical properties of injection-molded iron parts has been presented in a previous article.[11] However, no attempt was made in that study to examine the role of nickel in sintering kinetics. The objectives of this study were, therefore, to investigate how nickel affects the microstructure evolvement and sintering behavior of PIM iron parts and to correlate the sintering kinetics with the sintered densities of compacts made from different powders.

II. EXPERIMENTAL PROCEDURE

Carbonyl iron powder was selected as the base powder in this study. It has a spherical shape and an average diameter of 5.0 μm. For nickel additions, two different types of powders were used: a 5.3-μm carbonyl nickel powder

K.S. HWANG, Professor, is with the Institute of Materials Science and Engineering, National Taiwan University, Taipei, Taiwan, 106, Republic of China. M.Y. SHIAU, Senior Engineer, is with the Team Young Advanced Ceramics Co. Ltd., Taoyuan, Taiwan, 320, Republic of China.

Manuscript submitted June 26, 1995.

Table I. Characteristics of Iron and Nickel Powders Used in This Study

Powder type		iron	nickel 1	nickel 2
Designation		CIP-S-1641	Ni-123	HDNP
Vendor		ISP Corp. (Wayne, NJ)	International Nickel Co. (Toronto)	
Chemistry	C	0.78	0.06	0.07
	N	0.68	0.17	—
	O	0.92	0.19	0.05
	Fe	>97	—	---
Average particle size (Fisher subsieve sizer, ASTM B-330)		5.0 μm	5.3 μm	15.5 μm
Repose angle (α)		50 deg	55 deg	40 deg

with a spiky morphology (designated as Ni-123) and a 15.5-μm spherical nickel powder (designated as HDNP). The characteristics of these powders are given in Table I.

A replacement reaction method was employed in making Fe-Ni composite powders. Four compositions were examined in this study: 2, 4, 6, and 8 wt pct Ni. For each 100 g of iron powder, the calculated amount of nickel chloride ($NiCl_2 \cdot 6H_2O$) and 1.5 g of boric acid (H_3BO_3) were dissolved first in 800 cm^3 deionized water. After complete dissolution of the chemicals, iron powder was added into the solution. Hydrochloric acid was then added to trigger the replacement reaction while the powder and the solution were being stirred. The acidity of the solution was controlled in a range between pH3.5 and pH4.5, and the temperature was maintained between 70 °C and 80 °C.

Reacted composite powders were washed, filtered, dried, ground with a mortar and pestle to break up the agglomerates, and then sieved. The −325 mesh powders were saved for this study and were reduced in hydrogen at 450 °C for 2.5 hours. Reduced powders which were lightly sintered were then reground and resieved to −325 mesh.

The selected binder consisted of 44.4 wt pct polyethylene, 44.4 wt pct Acrawax*C (Ethcylenebisstearamide), and 11.2 wt pct stearic acid. This multicomponent binder was mixed with metal powders in an Σ-blade kneader. The powder loading was 92 wt pct (58.3 vol pct). The kneaded feedstock was then injection molded at 140 °C into tensile bar specimens. Molded samples were thermally debound using a stepwise heating schedule with the maximum temperature of 450 °C and a total debinding time of 38 hours. Due to the poor green strength in debound compacts, a presintering step at 700 °C for 3 hours was added in the final stage of the debinding cycle in order to avoid damages due to handling.[14] After debinding, specimens were sintered at 1200 °C for 1 to 3 hours. Since carbon influences significantly the sintering behavior and mechanical properties of PIM compacts, all debinding and sintering was conducted under hydrogen atmosphere to remove carbon so that the role of nickel could be identified exclusively.

To examine the sintering behavior of tensile bars, 15-mm gage length sections of tensile bars were cut off for dilatometry analysis. These specimens were thermally debound in hydrogen to remove all binder prior to the dilatometry tests. In dilatometer runs, the specimens were heated and cooled at a rate of 10 °C/min and were sintered at 1200 °C for 3 hours.

*ACRAWAX is a trademark of Glyco, Inc., Norwalk, CT.

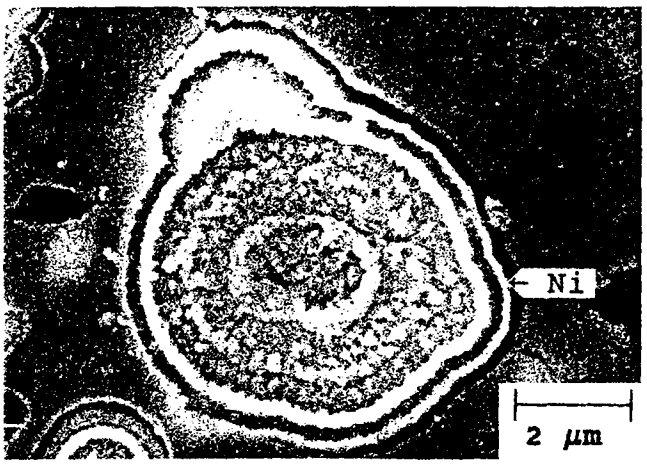

(a)

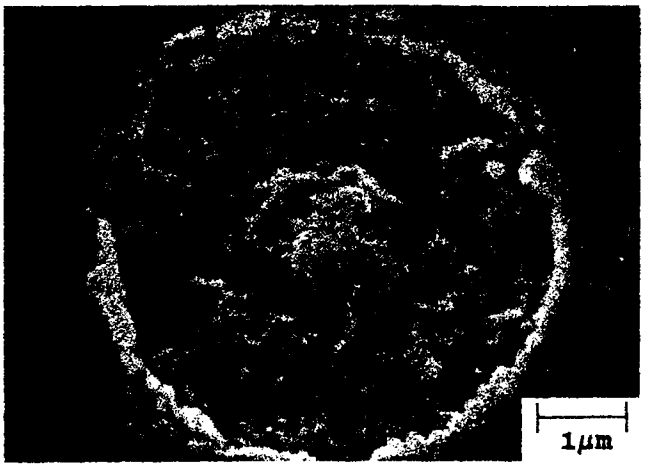

(b)

Fig. 1—The cross section of Fe-8 Ni composite powder (*a*) in the as-plated form and (*b*) in the plated-and-reduced form.

To understand the microstructure evolution during heating and sintering, samples were pulled out to the cooling zone of the furnace from different heating stages. The microstructure of the specimens was examined by using both an optical microscope and a scanning electron microscope (SEM). To study the homogeneity of nickel alloying, an electron probe microanalyzer (EPMA) was applied to detect the presence and distribution of nickel.

III. RESULTS

A. *Characteristics of Composite Powder*

Figures 1(a) and (b) are the cross sections of Fe-Ni composite powders in the as-plated and plated-and-reduced (450 °C, 2.5 hours, −325 mesh) forms, respectively, showing a uniform nickel layer about 0.2-μm thick. Inside the powder, the typical onion-layer structure was still present in the as-plated powder (Figure 1(a)), but it disappeared after hydrogen reduction (Figure 1(b)). Figure 2(a) shows that the surface of the reduced Fe-8Ni composite powder became rougher due to the coating treatment, but that it

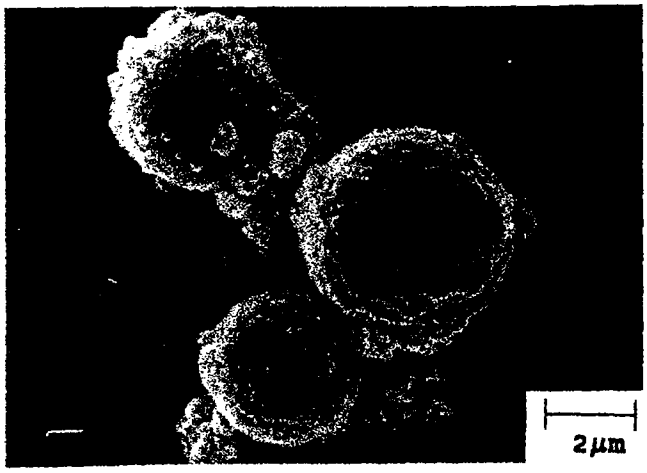

(*a*)

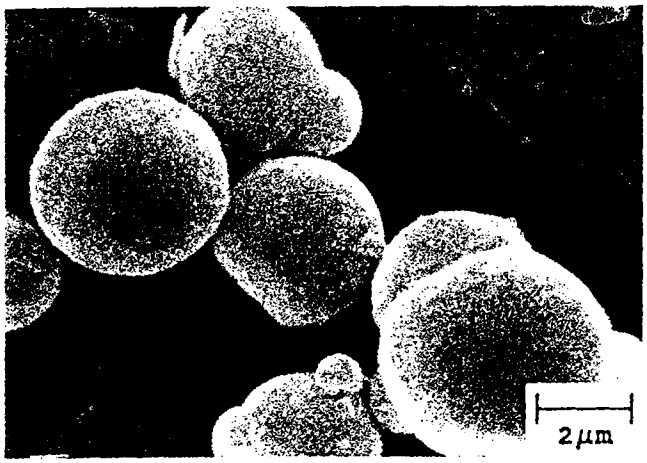

(*b*)

Fig. 2—The surface morphology of (*a*) Fe-8Ni reduced composite powder and (*b*) as-received iron powder.

Table II. The Nickel Content in the Fe-Ni Composite Powder as Measured by an Atomic Absorption Analyzer

Composite Powder	Measured Ni Content (Wt Pct)
Fe-2Ni	1.98
Fe-4Ni	3.96
Fe-6Ni	6.10
Fe-8Ni	7.94

remained spherical in shape, similar to that of the as-received iron powder, as shown in Figure 2(b). Table II gives the true nickel contents as measured by the atomic absorption analyzer. They are very close to the calculated values.

B. *Carbon Analysis*

Since carbon content influences significantly the sintering behavior of iron powder and affects evaluation of the role of nickel, the amount of carbon was monitored throughout the process using a LECO* CS-244 carbon analyzer. It dropped from the as-received 0.779 wt pct to 0.044 wt pct after hydrogen reduction and was further reduced to 0.006 wt pct after debinding. The sintered specimens contained 0.005 wt pct carbon. The role of nickel in sintering Fe-Ni compacts could thus be unequivocally established.

*LECO is a trademark of LECO Corporation, St. Joseph, MI.

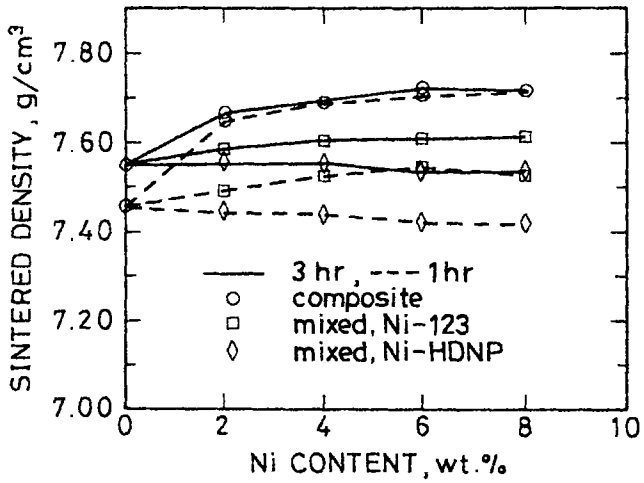

Fig. 3—Sintered densities of PIM parts which were made from composite and mixed Fe-Ni powders and were sintered at 1200 °C for 1 and 3 h, respectively.

C. *Density*

Figure 3 shows the sintered densities of specimens made from composite and mixed powders. These densities were measured by using the Archimedes method. The highest density, 7.72 g/cm³, was obtained by sintering Fe-6Ni composite powder for 3 hours. It is noteworthy that the sintering times, 1 and 3 hours, made little difference in the final sintered density for composite powders. It is also shown that 2 wt pct nickel was efficient enough in increasing the sintered density of the composite powders. Additional nickel resulted in little improvement. For mixed powders, fine Ni-123 nickel powder increased the sintered density slightly. However, when coarse HDNP nickel powder was used, the sintered density decreased slightly with increasing nickel content.

D. *Dilatometry Analysis*

Figure 4 shows the amount of shrinkage and the shrinkage rate of debound compacts in a dilatometer run. It is seen that sizable shrinkage of the pure iron compact started at 800 °C and that the shrinkage rate reached a maximum at 912 °C, where the alpha-gamma phase transformation occurred. After phase transformation, the diffusion rate decreased while grain size increased substantially, which slowed down the shrinkage rate.[15,16] As the sintering temperature continued to increase, the shrinkage rate reached another peak at 1170 °C.

For Fe-8Ni compacts made from either composite or elemental mixed powders, no obvious transformation temperature was observed at 912 °C. This indicated that there was very little pure iron in the Fe-8Ni compacts because interdiffusion of Fe-Ni had occurred during thermal debinding and at the heating-up period of the dilatometer run. As a result, the phase transformation temperature decreased

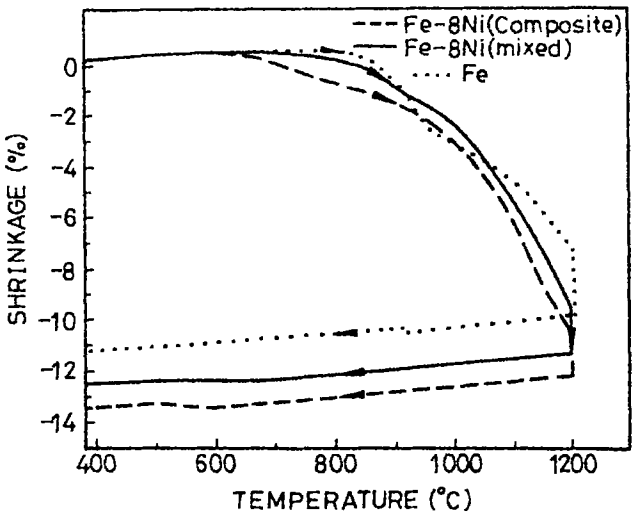

(*a*)

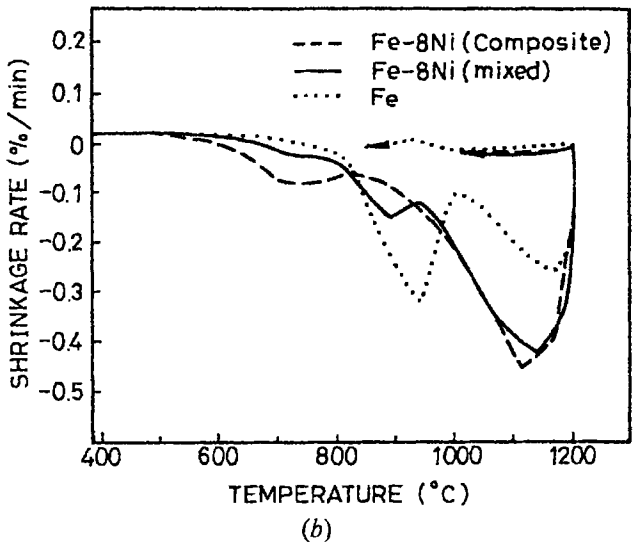

(*b*)

Fig. 4—Dilatometer curves showing the (*a*) shrinkage and (*b*) shrinkage rate of Fe and Fe-8Ni compacts made from composite and mixed powders.

due to nickel alloying, as suggested in Figure 5 of the Fe-Ni phase diagram.[17] Moreover, as phase transformation occurred, it did not take place at a fixed temperature because the material was not yet homogenized.

E. *Metallography*

To help explain the dilatometric curves discussed in Section D, SEM examination on the microstructure evolution during heating was conducted. Figures 6 and 7 show the microstructures of pure iron, mixed Fe-8Ni, and composite Fe-8Ni powder compacts which were pulled out of the furnace as soon as the temperature reached 800 °C and 900 °C, respectively.

Figure 6(a) shows that sintering signs, such as neck formation, were already present at 800 °C for pure iron compacts. However, individual particles were still discernible. As sintering temperature increased to 900 °C, the grain size and neck size became much larger and individual particles were no longer discernable, as shown in Figure 7(a). Figures 6 and 7 also show that Fe-8Ni compacts made from composite powders underwent little sintering at low temperatures. Individual Fe-Ni composite powders were still distinguishable, and the cusps at the contact region were still very sharp even after being heated to 900 °C. Figures 6(b) and 7(b) also show a contour sharper than that of the pure iron powder. This indicated that Fe-Ni alloy had formed at the outer layer and was harder and more resistant to etchant attack.

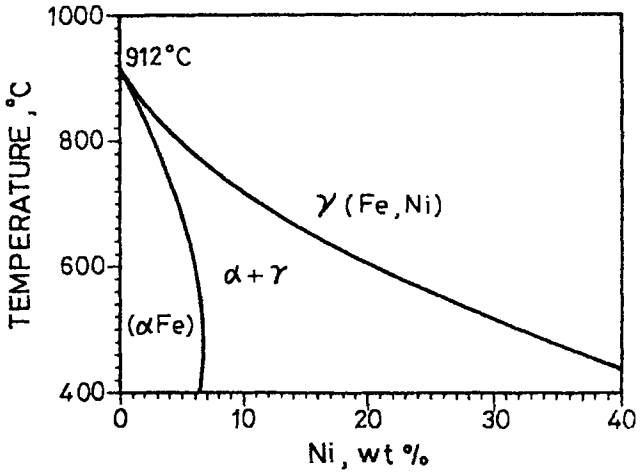

Fig. 5—Fe-Ni phase diagram showing the decreasing phase transformation temperature and wider gamma + alpha zone with increasing nickel content.[17]

For those parts made from coarse HDNP nickel powders, nonuniform microstructures at 900 °C were observed. Figure 7(c) shows that a very high density area was present. The EPMA analysis showed that this region was rich in nickel, indicating that this area was the original nickel powder site. Surrounding this area, larger pores were present. In addition, sharp powder edges similar to the composite powder observed in Figure 7(b) were found. This suggested that an appreciable amount of nickel was deposited on iron powder surfaces, possibly through the surface diffusion.

For grain size comparisons, optical metallographs were prepared for Fe and Fe-8Ni compacts which were sintered at 1200 °C for 1 hour. It is seen in Figure 8(b) that grains in the composite powder compacts were smaller and more irregular than pure iron specimens, as shown in Figure 8(a). As sintering time increased to 3 hours, the composite powder specimens (Figure 9(b)) showed similar grain size but still appeared more irregular in shape compared to the pure iron compacts (Figure 9(a)). For mixed powders sintered for 3 hours, Figures 9(c) and (d) show a nonuniform microstructure with a small grain iron matrix surrounding nickel-rich sites, which can be identified by the grain boundary free areas due to their resistance to etchant attack. These observations support the previous findings[1,2,9,10,18] that the presence of nickel in the grain boundaries of iron powder impedes grain growth.

Figure 9(d) also shows that large pores were present when coarse HDNP nickel powder was used. Thus, even with fine grains in the compact and locally dense regions in the matrix, the overall sintered density of some mixed Fe-Ni powders decreased with an increasing amount of nickel, as shown in Figure 3.

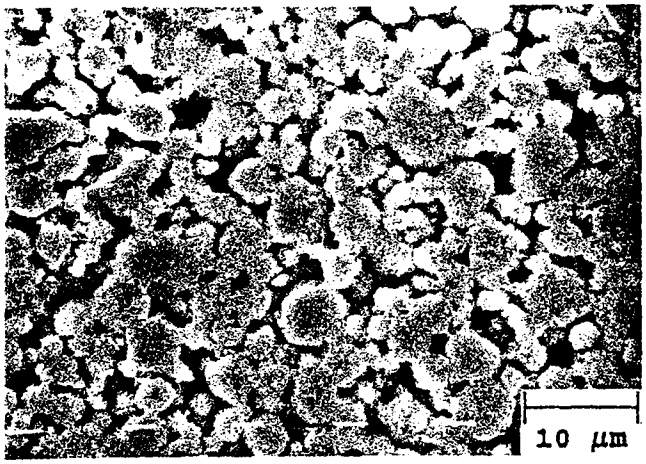

(a)

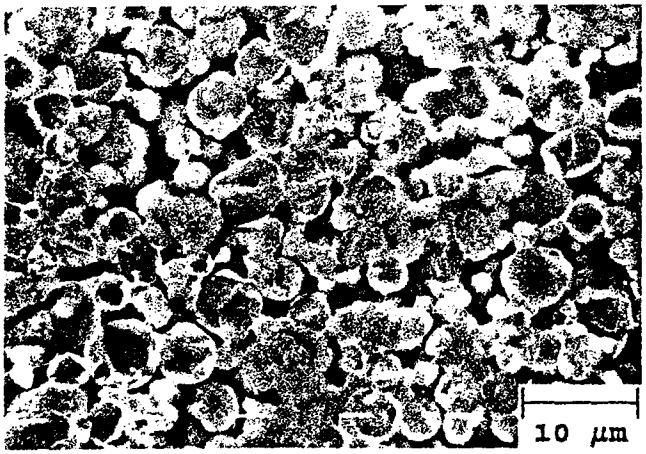

(b)

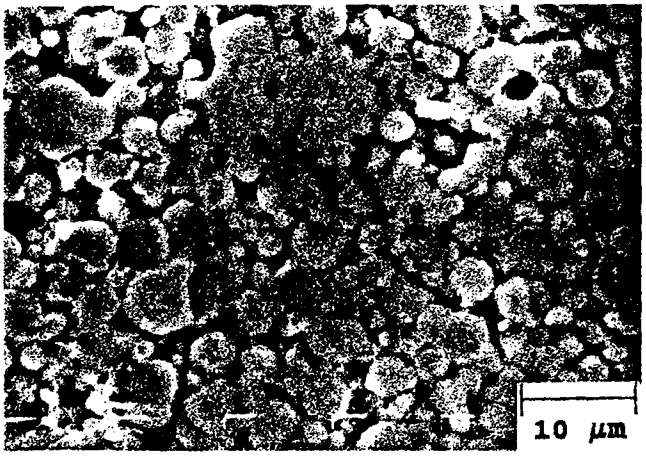

(c)

Fig. 6—SEM pictures of samples removed at 800 °C during heating: (*a*) Fe, (*b*) Fe-8Ni made from composite powder, and (*c*) Fe-8Ni made from HDNP nickel powder.

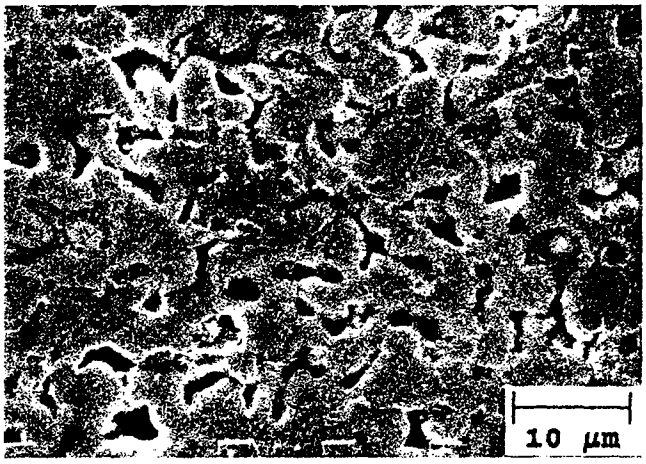

(a)

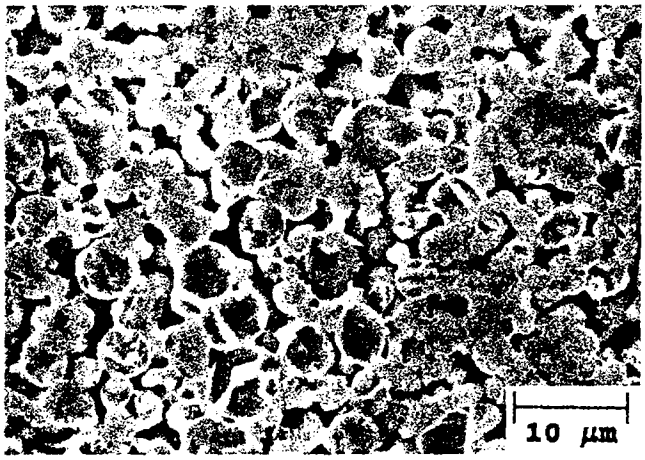

(b)

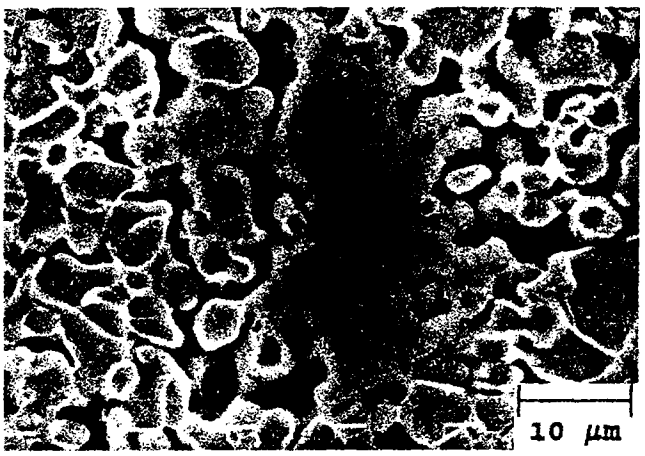

(c)

Fig. 7—SEM pictures of samples removed at 900 °C during heating: (*a*) Fe, (*b*) Fe-8Ni made from composite powder, and (*c*) Fe-8Ni made from HDNP nickel powder.

F. *Degree of Homogenization*

It is seen from the microstructures in Figure 9 that the composite powder had a faster homogenization rate compared to the mixed powders. Results of line scan and X-ray mapping of nickel conducted under EPMA for composite powder compacts which were sintered at 1200 °C for 1 hour showed that there were no nickel-rich areas after sintering. On the other hand, the nickel distribution in sintered Fe-8Ni compacts made from HDNP powders was not uniform. Figure 10 shows the line scan of the nickel element using EPMA. The highest nickel content at the center of the nickel-rich region amounts to 83 wt pct.

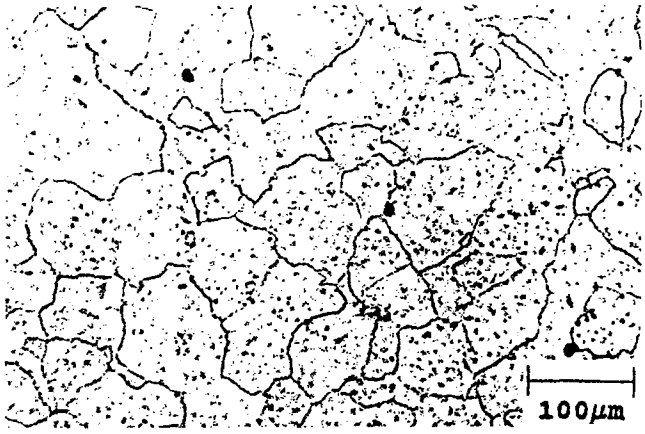

(*a*)

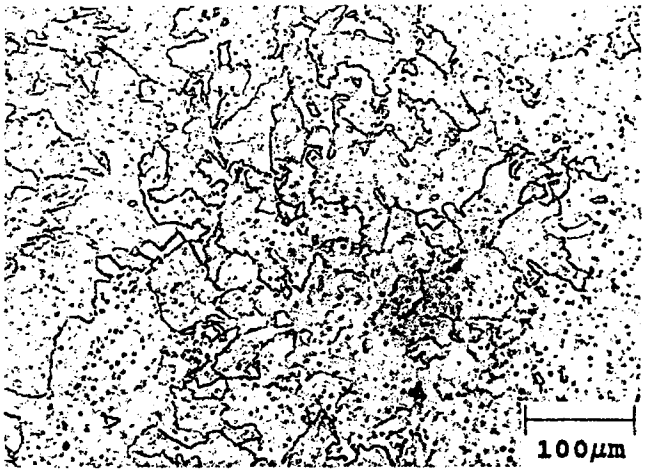

(*b*)

Fig. 8—Optical micrographs of specimens sintered at 1200 °C for 1 h: (*a*) Fe and (*b*) Fe-8Ni made from composite powder.

IV. DISCUSSION

A. *Effect of Nickel on Neck Growth*

Previous studies have shown that surface diffusion is the dominant sintering mechanism for iron[19–22] but that it does not contribute to densification. This phenomenon was also observed in this study, as illustrated in Figures 4 and 7(a), in which large necks were observed with little densification. Contrary to pure iron powders, much less neck growth was noticed on Fe-Ni composite powders, as shown in Figure 7(b). Since both pure iron and Fe-8Ni have about the same amount of shrinkage at 900 °C, as illustrated in Figure 4, the comparison of the neck size indicated that the surface diffusion of iron was impeded in composite powders. Consequently, most driving forces, *i.e.*, surface area, for sintering are preserved at low temperatures for composite powder compacts. These driving forces are then used at high temperatures where the relative role of densification mechanisms, *i.e.*, grain boundary diffusion and volume diffusion, is greater than at low temperatures.

This retardation in neck growth is very likely because the surface diffusion coefficient of nickel is much smaller than that of iron, particularly between 800 °C and 912 °C, as shown in Figure 11.[23,24] Thus, the difference in neck size and grain size between pure iron and Fe-Ni composite powder compacts was most significant around 900 °C, as demonstrated in Figures 7(a) and (b). It could be argued that nickel would be homogenized with iron in the sintering process. This homogenization, however, did not occur, as was indicated by the sharp contours on powders shown in Figures 6(b) and 7(b). Moreover, even a compact which was homogenized gave a low surface diffusion rate because homogenized Fe-8Ni transformed at temperatures as low as 760 °C (Figure 5) into the gamma phase. As Fe-8Ni compacts change from alpha to gamma phase, a drop in the surface diffusion coefficient is expected, as is the case of pure iron for which a factor of 8 decrease was reported.[24] Thus, less neck growth was observed between 700 °C and 912 °C in the Fe-Ni compact.

Previous studies have shown that whether exaggerated grain growth occurred during heating determined whether high sintered densities could be obtained for carbonyl iron compacts.[15,16] Thus, the microstructure evolvement before 1200 °C was reached is critical. Therefore, the factors, particularly the neck size and the nickel distribution, which could influence the grain growth were monitored. Figure 12(a) represents the case for Fe-Ni which has smaller necks at 900 °C than those of pure iron materials, as shown in Figure 12(b). As grain growth proceeds, in order to reduce the total grain boundary area, the grain boundary tends to move toward the neck but will be stopped at the interparticle contact where the grain boundary area is the smallest. For further growth, a greater chemical driving force would be needed compared to the case of pure iron with a large neck. Thus, a small neck size would be favorable for retarding the grain growth.

Another probable effect of nickel addition is that the specimens are not yet homogeneous during heating, which forces phase transformation to occur at different temperatures in different regions within the compact. As a result, both alpha and gamma phases coexist during heating, which impedes exaggerated grain growth during phase transformation. In the case of Fe-Ni composite powders, the presence of nickel at the particle contacts also adds another barrier to the movement of growing grains.

B. *Pore Structure Evolution*

Previous diffusion couple experiments have shown that the volume diffusion of Ni into Fe is slower than that of Fe into Ni and Fe-Ni alloys.[2,25,26] Thus, Kirkendall pores, if present, should occur on the iron powder side. However, Figure 9(d) shows that unusually large pores were present in nickel-rich areas as identified by EPMA analysis. It is postulated here that most of these pores were not formed directly from vacancy coalescence due to the Kirkendall effect but were formed due to particle rearrangement. This is because when the Kirkendall effect occurred, the iron powder which suffered a loss of mass tended to shrink in the direction of interdiffusion and was placed under tensile stresses.[27,28] It is very likely that this shrinkage force and these stresses could cause particle rearrangement of the neighboring iron powders and result in large interparticle pores around nickel particles. This phenomenon seemed to be more pronounced when nickel was less uniformly distributed, as in the case with the large HDNP nickel powders

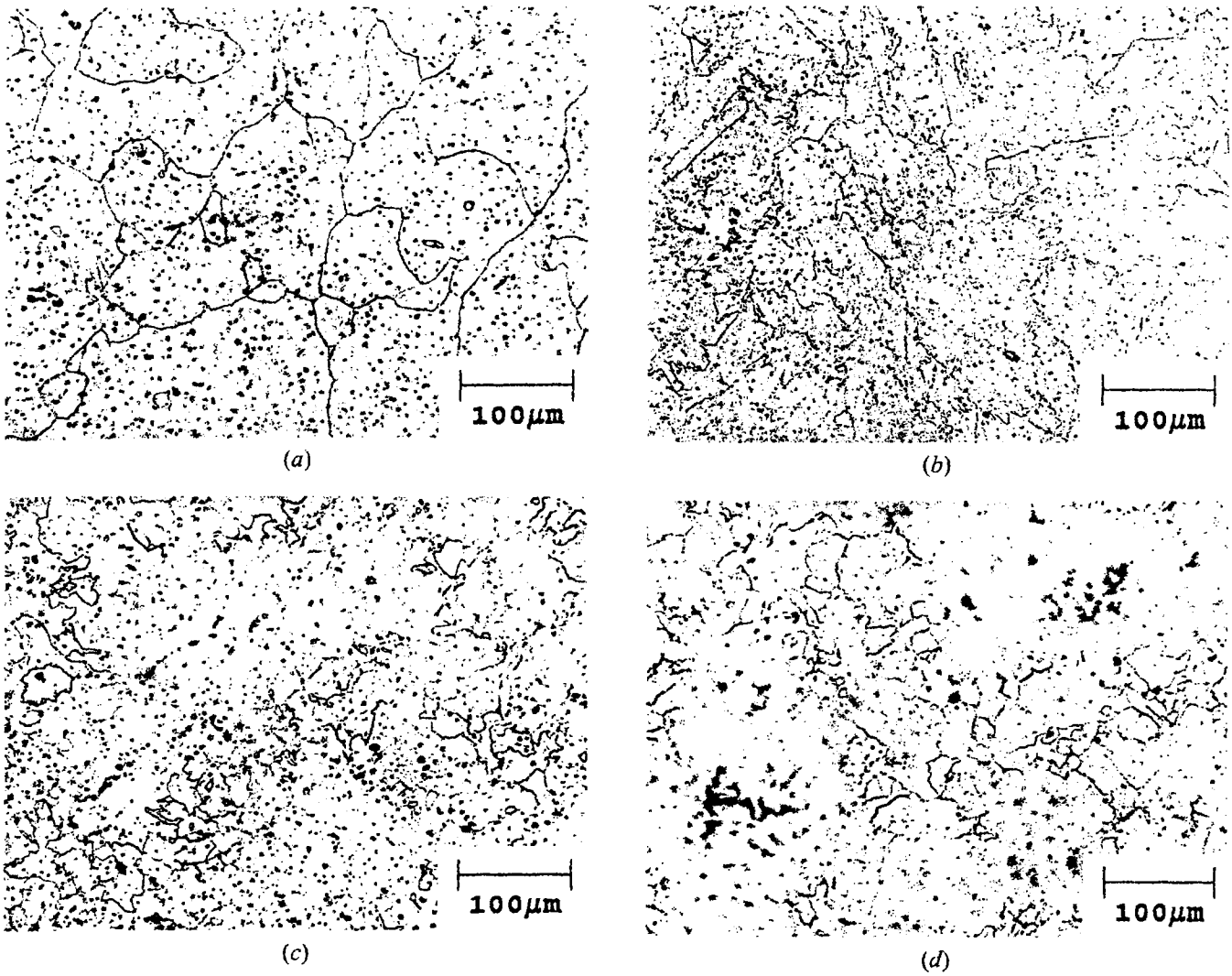

Fig. 9—Optical micrographs of samples sintered at 1200 °C for 3 h: (*a*) Fe, (*b*) Fe-8Ni made from composite powder, (*c*) Fe-8Ni made from Ni-123 nickel powder, and (*d*) Fe-8Ni made from HDNP nickel powder.

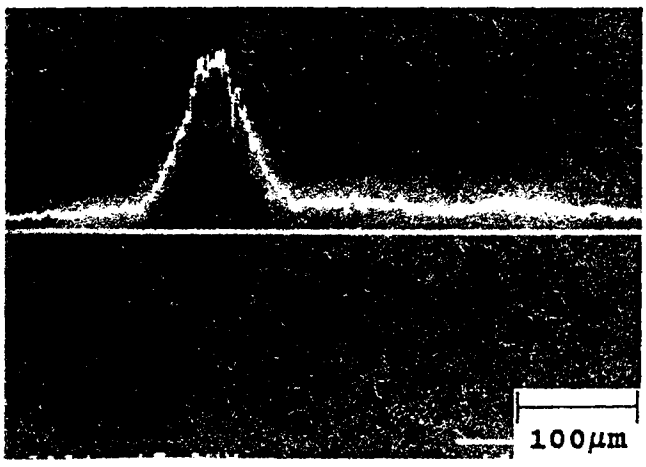

Fig. 10—A line scan for nickel content conducted on sintered Fe-8Ni parts made from HDNP nickel powders.

shown in Figure 7(c). As sintering proceeded, these pores became too large to be removed and became trapped within the dense area, as shown in Figures 9(c) and (d).

It was shown in several previous studies that the amount of shrinkage of composite powder compacts increased with increasing nickel content for the range of nickel which was also investigated in this study. This trend was, however, influenced by the iron powder used. For large size iron powders, the degree of sintering enhancement was lessened because there was less powder surface available for nickel coating for promotion of sintering. An example is given by Hanatate *et al.*,[10] who showed that the optimum amount of nickel coating for −150 + 200 mesh (−106 + 75 μm) electrolytic iron powder was 0.08 wt pct. Over 0.08 wt pct, the amount of shrinkage of a powder compact with nickel-coated iron powder became constant. An expansion was even observed when 5 wt pct Ni was coated on 170-μm large iron powders because of the nickel diffusion into iron grain boundaries.[18]

C. *Diffusion Mechanisms*

Several studies have indicated that the elimination of porosity in iron compacts is mainly due to grain boundary diffusion.[29,30] It has been shown that the grain boundary

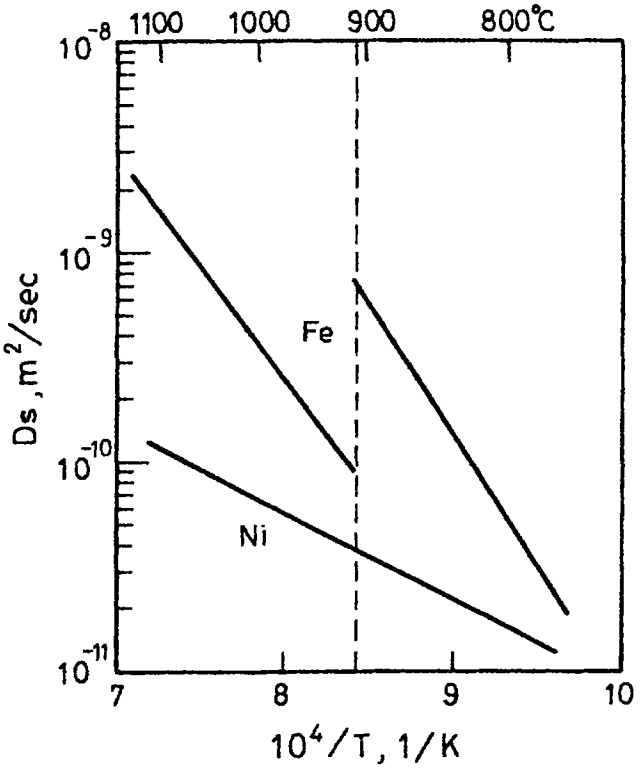

Fig. 11—The surface diffusion coefficients of iron and nickel.[23,24]

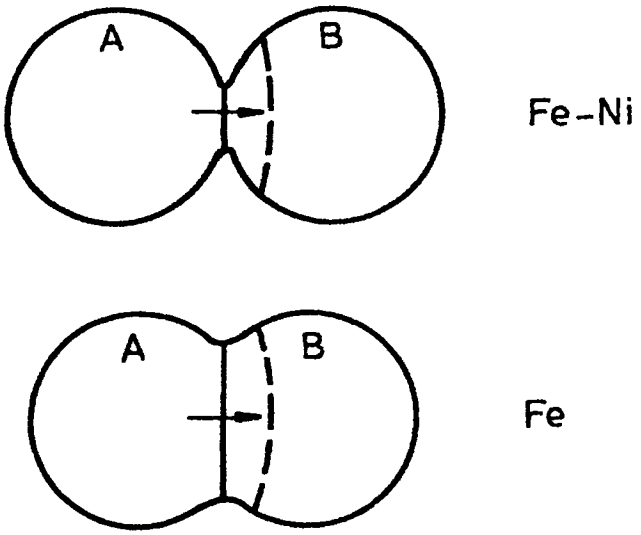

Fig. 12—Schematics showing the difference in the energy barrier for grain boundaries to break away from the contact area with different neck sizes: (*a*) sharp neck and (*b*) blunted neck.

diffusion rate of iron is enhanced by the presence of nickel.[10] This suggests that grain boundaries which contain nickel will become short-circuit diffusion paths for iron diffusion during sintering.[9] Thus, how to introduce nickel effectively into iron becomes critical in enhancing the densification of iron compacts. It is obvious that the best method is to coat nickel directly onto the iron particle surfaces so that the nickel can penetrate more effectively into the grain boundaries inside the iron powder. This method gives more uniform nickel distribution and shorter diffusion distance for iron to reach the short-circuit path.

For the Fe-Ni mixed powder system, enhanced sintering is still observed compared to the results with pure iron compacts. Although nickel is not uniformly distributed on iron powder surfaces in green compacts, it can still penetrate into iron quickly through surface and grain boundary diffusion during sintering.[10,12,31] Thus, some densifications in mixed Fe-Ni powders can still occur, depending on the particle size of the iron and nickel powders.

V. CONCLUSIONS

Nickel is a strong sintering aid for powder-injection-molded iron parts, particularly when it is added in the composite powder form. It was observed in the composite powder compacts that nickel additions slowed down the neck growth rate of iron powders in the early sintering stage. The dilatometer runs indicated that nickel was not yet homogenized into iron during heating, so that both alpha and gamma phases coexisted before 912 °C was reached due to nonuniform phase transformation. It is suggested that this dual-phase microstructure, small neck size, and presence of nickel at particle contacts suppressed exaggerated grain growth, which usually occurs in pure iron compacts at 912 °C. As a result, the Fe-Ni composite powder compacts sintered at 1200 °C for 1 hour showed finer grains and higher sintered densities compared to results with pure iron compacts.

When nickel was added in the mixed powder form, local densification was obtained for the same reasons as it was with composite powder. However, large pores also formed around nickel powders because of particle rearrangement caused by the Kirkendall effect. These large pores became trapped inside the grains and were difficult to remove even after 3 hours of sintering at 1200 °C. Both expansion and shrinkage were observed in this study; which one occurred depended on the particle size and the method of nickel introduction.

ACKNOWLEDGMENTS

We are grateful for the support of this work by the National Science Council of the Republic of China under Contract No. NSC80-0405-E-002-28.

REFERENCES

1. L. Forss: in *Perspectives in Powder Metallurgy*, vol. 3, *Iron Powder Metallurgy*, H.H. Hausner, K.H. Roll, and P.K. Johnson, eds., Plenum Press, New York, NY, 1968, pp. 211-20.
2. H. Mitani, Y. Hanatate, and K. Majima: *J. Jpn. Inst. Met.*, 1976, vol. 48, pp. 903-08.
3. I.M. Fedorchenko and I.I. Ivanova: in *Modern Developments in Powder Metallurgy*, H.H. Hausner, ed., Plenum Press, New York, NY, 1966, vol. 2, pp. 26-43.
4. H. Zhang and R.M. German: *Int. J. Powder Metall.*, 1991, vol. 27, pp. 249-54.
5. H. Zhang, R.M. German, K.F. Hens, and D. Lee: *Powder Metall. Int.*, 1990, vol. 22, pp. 15-18.
6. S.T. Lin and R.M. German: in *Advances in Powder Metallurgy*, compiled by E.R. Andreotti and P.J. McGeehan, MPIF, Princeton, NJ, 1990, vol. 3, pp. 423-35.
7. F.V. Lenel and K.S. Hwang: *Powder Metall. Int.*, 1980, vol. 12, pp. 88-90.
8. E. Friedrich, K.P. Wieters, and O. Chehade: in *Advances in Powder*

Metallurgy and Particulate Materials, compiled by J.M. Capus and R.M. German, MPIF, Princeton, NJ, 1992, vol. 3, pp. 85-98.
9. S. Kohara and K. Tatsuzawa: *J. Jpn. Powder Powder Metall.*, 1984, vol. 31, pp. 183-88.
10. Y. Hanatate, K. Majima, and H. Mitani: *J. Jpn. Inst. Met.*, 1976, vol. 40, pp. 1010-15.
11. K.S. Hwang and M.Y. Hsiao: in *Powder Injection Molding Symp.*, P.H. Booker, J. Gaspervich, and R.M. German, eds., MPIF, Princeton, NJ, 1992, pp. 53-66.
12. H. Mitani, Y. Hanatate, and K. Majima: *J. Jpn. Inst. Met.*, 1976, vol. 40, pp. 903-08.
13. Y. Hanatate, M. Yamamoto, and H. Mitani: *J. Jpn. Inst. Met.*, 1977, vol. 41, pp. 1211-16.
14. K.S. Hwang and T.H. Tsou: *Metall. Trans. A*, 1992, vol. 23A, pp. 2775-82.
15. G. Cizeron and P. Lacombe: *C. R. Acad. Sci.*, 1955, vol. 241, pp. 409-10.
16. F.V. Lenel, G.S. Ansell, and J.R. Strife: in *Modern Developments in Powder Metallurgy*, H.H. Hausner and W.E. Smith, eds., 1974, vol. 6, pp. 275-92.
17. O. Kubaschewski: *Iron-Binary Phase Diagrams*, Springer-Verlag, Berlin, 1982, pp. 73-78.
18. J. Puckert, W.A. Kaysser, and G. Petzow: *Int. J. Powder Metall. Powder Technol.*, 1984, vol. 20, pp. 301-10.
19. H.F. Fischmeister and R. Zahn: in *Modern Developments in Powder Metallurgy*, H.H. Hausner, ed., Plenum Press, New York, NY, 1966, vol. 2, pp. 12-25.
20. A.R. Poster and H.H. Hausner: in *Modern Developments in P/M*, H.H. Hausner, ed., Plenum Press, New York, NY, 1966, vol. 2, pp. 26-43.
21. H. Ichinose and H. Igarashi: *J. Jpn. Powder Powder Metall.*, 1989, vol. 36, pp. 352-56.
22. F.B. Swinkels and M.F. Ashby: *Acta Metall.*, 1981, vol. 29, pp. 259-81.
23. J.M. Blakely and H. Mykura: *Acta Metall.*, 1961, vol. 9, pp. 23-31.
24. J.M. Blakely and H. Mykura: *Acta Metall.*, 1963, vol. 11, pp. 399-04.
25. B. Million, J. Ruzickova, J. Velisek, and J. Vrestal: *Mater. Sci. Eng.*, 1981, vol. 50, pp. 43-52.
26. J.I. Goldstein, R.E. Hanneman, and R.E. Ogilvie: *Trans. TMS-AIME*, 1965, vol. 233, pp. 812-20.
27. R.E. Reed-Hill and R. Abbaschian: *Physical Metallurgy Principles*, 3rd ed., PWS-KENT Publishing Co., Boston, MA, 1992, pp. 368-69.
28. J.A. Brinkman: *Acta Metall.*, 1955, vol. 3, pp. 140-45.
29. J.J. Bacmann and G. Cizeron: *Int. J. Powder Metall.*, 1969, vol. 5, pp. 39-53.
30. R.M. German: *Powder Metallurgy Science*, Metal Powder Industries Federation, Princeton, NJ, 1984, p. 173.
31. P.F. Stablein, Jr. and G.C. Kuczynski: *Acta Metall.*, 1963, vol. 11, pp. 1327-37.